ChemPubSoc Europe

DOI: 10.1002/cphc.201800284

CHEMPHYSCHEM Articles

Behavior of a Metal Organic Framework Thin-Film at Elevated Temperature and Pressure as Studied with an Autoclave-Inserted Atomic Force Microscope

Rogier P. Brand[+],[a] Laurens D. B. Mandemaker[+],[a] Guusje Delen,[a] Niek Rijnveld,[b] and Bert M. Weckhuysen*[a]

Bridging the gap in studying surface reactions, processes, and morphology and measuring at (catalytic) relevant conditions is crucial for our understanding of the working principles of porous crystalline materials. Scanning tunneling microscopy is limited because of the required conductivity of the sample, whereas atomic force microscopy (AFM) is often challenging in use owing to the physical mechanism underlying the technique. Herein, we report a tailor-made autoclave-inserted AFM, able to measure at ~20 bar and ~110 °C. First, we show the ability to obtain nanometer resolution on well-defined test samples at before-mentioned conditions. Second, to demonstrate the possibilities of analyzing morphological evolutions at elevated temperatures and pressures, we use this setup to measure the stability of a surface-anchored metal-organic framework (SURMOF) in-situ at pressures of 1–20 bar in the temperature range between 20 and 60 °C. It was found that the showcase HKUST-1 material has a good physical stability, as it is hardly damaged from exposure to pressures up to 20 bar. However, its thermal stability is weaker, as exposure to elevated *T* damaged the material by influencing the interaction between organic linker and metal cluster. In-situ measurements at elevated *T* also showed an increased mobility of the material when working at such conditions. Combining the strength of AFM at elevated *T* and *p* with ex-situ AFM and spectroscopic measurements on this MOF showcases an example of how porous materials can be studied at (industrially) relevant conditions using the autoclave-inserted AFM.

1. Introduction

The discovery of scanning probe microscopy (SPM) and more specifically atomic force microscopy (AFM)[1,2,3] have led to many possibilities in studying surfaces, and their characteristics at the (sub-)nanometer scale.[4] Although it was at first mostly applied in physics and biology,[5–11] SPM techniques gradually find their way to other fields, such as chemistry, functional materials science as well as heterogeneous catalysis. Until recently most (commercial) SPM instruments were designed for operation in ultra-high vacuum or at ambient *p* and in a *T* range from −269 °C to room temperature. Therefore, in-situ applications with a combination of elevated *T* and *p* – of particular interest in heterogeneous catalysis research – were previously not possible.

However, progress has been made, for instance by the Rimer group using liquid-phase AFM to investigate the growth of silicalite crystals at elevated *T*.[12,13] Another example includes the Frenken group, that has performed advanced studies on scanning tunneling microscopy (STM) at high *T* and *p*,[14,15] and later even showcased an AFM system able to measure at similar conditions.[16] Their in-situ STM measurements on the CO oxidation and NO reduction over noble metal catalysts represent a glimpse of the large number of case studies possible using these advanced SPM methods.[17–20] Using AFM instead of STM bridges the material gap, as substrates don't necessarily have to be conductive for AFM measurements. This paves the way for detailed characterization studies of (partially) isolating solid catalyst materials, as their most relevant underlying mechanisms are often occurring on their surface.

Porous crystalline solids are an important class of heterogeneous catalysts with, for example, zeolites as one of the most prominent examples.[21,22] Metal-Organic Frameworks (MOFs) are an emerging class of crystalline porous solids that recently have received a lot of attention.[23–29] There are a several major reasons that MOFs are popular in (catalysis) research. These materials are comprised of metal cations and organic linkers. The facile interchangeability of both metal nodes and organic linkers in making up various MOFs makes them very versatile in (catalytic) functionality. Additionally, the pore- and cage sizes can easily be tuned by in-/decreasing the linker size and/or length. By specifically tailoring MOFs, intelligent catalyst design can be realized. A limiting factor in using MOFs for large-scale industrial catalytic processes is often a lack in (mechanical/

[a] R. P. Brand,[+] L. D. B. Mandemaker,[+] G. Delen, Prof. B. M. Weckhuysen
Debye Institute for Nanomaterials Science, Utrecht University
Universiteitsweg 99, 3584 CG Utrecht (The Netherlands)
E-mail: b.m.weckhuysen@uu.nl
[b] N. Rijnveld
Optics 11
De Boelelaan 1081, 1081 HV Amsterdam, The Netherlands
[+] These authors contributed equally to the work

Supporting information for this article is available on the WWW under https://doi.org/10.1002/cphc.201800284

hydrothermal) stability during reactions at elevated *T* and *p*. However, besides former studies using XRD, detailed information on the thermal and physical (morphological) stability of such MOFs is lacking.[30]

MOFs stabilized in the form of porous membranes are gaining popularity because of their possible applications and are simultaneously suitable as model systems for AFM studies. Such surface mounted MOFs, or SURMOFs, can be used as gas storage- and separation membranes, sensors and as catalytic surfaces.[31–34] These MOFs are anchored to a substrate, such as glass, SiO_2, Al_2O_3 and Au/Si. As an added benefit, by functionalizing a substrate surface with Self-Assembled Monolayers (SAMs) also their orientation, among other things, can be controlled. In this manner, for example, the alignment of pore channels with resulting decreased diffusion limitations can be realized. The molecules for SAMs on gold are typically thiols. The thiol group is in most cases linked by a hydrocarbon middle part to a terminating head group of specific functionality (e.g., hydroxyl, carboxylic acid and amine). These head groups function as nucleation points for SURMOF growth. Their chemistry, together with their surface density, direct the resulting orientation of the SURMOF.[35]

Within this context, HKUST-1, consisting of copper (II) ions and 1,3,5-BenzeneTriCarboxylate (BTC, and also known as trimesic acid) linkers, is one of the most studied (SUR)MOFs.[36,37] In both bulk and as a membrane several functionalities of HKUST-1, such as its gas sorption properties of N_2, H_2 and CO_2 have been studied extensively and have shown excellent prospects.[38–43] Importantly, a lot of research has been performed on optimizing the synthesis of HKUST-1 SURMOFs. An easy, albeit somewhat elaborate, synthesis procedure has been developed by Shekhah et al. to produce SURMOF thin-films in a highly controlled fashion by separating the growing stages of the metal ions and the organic linkers, known as the Layer-by-Layer (LbL) method (Figure 1b).[44–47] In this method, the SAM functionalized substrate is immersed alternately in the metal- and linker solution with washing steps in between these immersion cycles to assure the removal of excess surface (metal/linker) species between growth stages (Figure 1b).

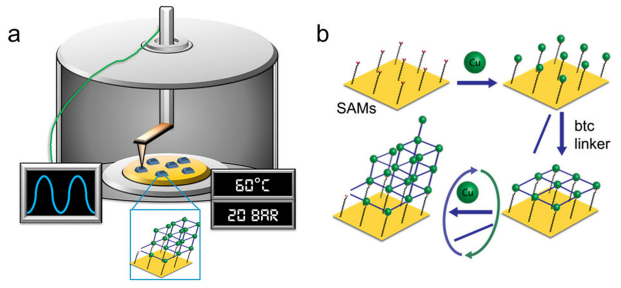

Figure 1. a) Schematic of the autoclave-inserted atomic force microscopy (AFM) measuring concept. The surface morphology of thin-films with HKUST-1 crystals grown by Layer-by-Layer (LbL) synthesis (b) placed in the autoclave-AFM is monitored. During AFM measurements, the temperature and pressure can be (simultaneously) increased up to 113 °C and 20 bar. b) Schematic of the LbL synthesis of HKUST-1 thin-films as a model system to investigate the potential of the in-situ AFM set-up. A Au/Si substrate is functionalized with Self-Assembled Monolayers (SAMs) and is alternately immersed in ethanolic copper (II) and BenzeneTriCarboxylic (BTC) solutions. In between deposition steps (Cu/BTC) the substrates are washed using pure ethanol. Layer thickness is determined by the amount of deposition cycle repetitions. Layer order is dependent on the degree of washing used.

Recent work by our group has studied the mechanism of HKUST-1 SURMOF formation using this LbL approach and has found a large significance of the washing step on the resulting metal organic framework thin-film quality.[48] For the work described below, it was of high relevance that individual grains of SURMOF were visible in AFM micrographs in order to monitor the effect of *T* and *p*. Therefore, the LbL synthesis procedure was adapted to use incomplete washing steps in order to grow inhomogeneous SURMOF surfaces. To study these MOF features, we present a new instrument, that is suitable to investigate the (changes in) surface morphology in-situ with AFM (in contact mode) up till ~20 bar and ~110 °C. To be able to do this, an AFM was integrated within an autoclave, with pressurizing (by using N_2 gas) and direct heating possibilities (Figure 1a). In this study, we first elucidate on the in-situ AFM and working conditions, and then demonstrate the ability to measure a relevant MOF thin-film sample under working conditions, analyzing the stability of a HKUST-1 SURMOF under elevated *T*, *p*, and a combination thereof.

2. Results and Discussion

2.1. Autoclave-Inserted Atomic Force Microscope

Integrating an AFM into an autoclave comes with several challenges. Increasing *T* and *p* influences the piezo crystals, cantilever and, naturally, the scanned sample. It is very difficult to use commercial scanning systems using a laser-deflection based setup, as changing *T*, *p*, gas environments, etc. would probably cause the need for constant refocusing of the laser on the cantilever and retuning of the resonance frequency. Instead, we used an interferometer-based scanning system, that exhibits very low noise and where the cantilever is always in focus of the laser beam. More details on the tailor-made autoclave-inserted AFM can be found in the Experimental Section. Figure 2 displays the schematics of the autoclave-inserted AFM and close-up pictures can be found in Figure S1. As can be seen from Figure 2, integrating the AFM inside an autoclave was done by housing the AFM tip into the head of the autoclave, and the base held the scanning piezo crystals while a membrane closed the system connecting the sample holder and base.

To show that the system is able to scan at increased T and p, a commercial TGZ2 sample (normally used for calibrations), consisting of a Si wafer and SiO_2 substrate, was scanned at elevated conditions (Figure 3a). This substrate has a high thermal stability and low thermal expansion coefficient, making it ideal to compare the resolution of the AFM at different conditions. As can be seen for the scans at elevated *T* and *p*, the scanning resolution in height is hardly influenced by the conditions, as the height differences are minimal under different *T* and *p* conditions. The width of the bar is ~1.5 μm, and as can be seen, the scans performed at different *p* slightly vary,

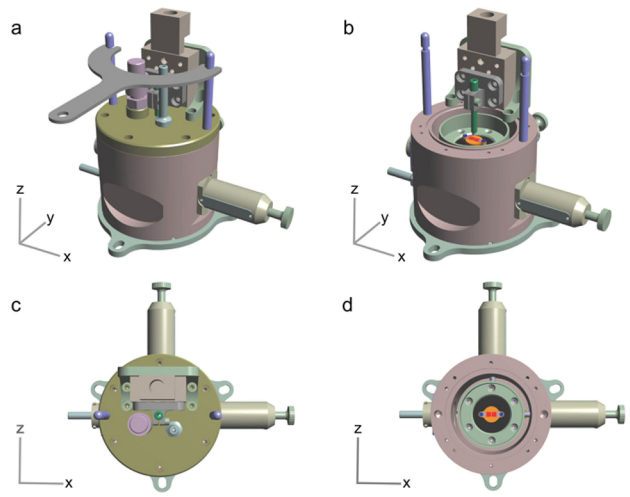

Figure 2. Schematics of the autoclave AFM cell in different configurations and perspectives: a) Complete system showing the cell in closed configuration. b) Similar representation, but without lid, showing the probe (green) in its holder and the sample (orange). c,d) Top views of (a) and (b), respectively. The sample (red) is fixated by two clamps on the sample table. The sample table is mounted on the sample stage, via magnet in the stage and a three-pin connection to avoid rotation. This sample holder is positioned in the middle of a cup like reservoir (green grey) with a temperature and pressure resistant membrane (black). Coarse lateral positioning is possible using the perpendicular large coarse screws (yellow grey) at the outside of the cell shown in all figures. The head consists of a lid (gold) which can be closed with screws. On the lid is the probe holder (grey), holding the probe (green), as well as a temperature controller (purple) and gas inlet (greyish green). The whole head can be fixed at a higher position on the pillars (purple) with the fork (grey) when exchanging samples.

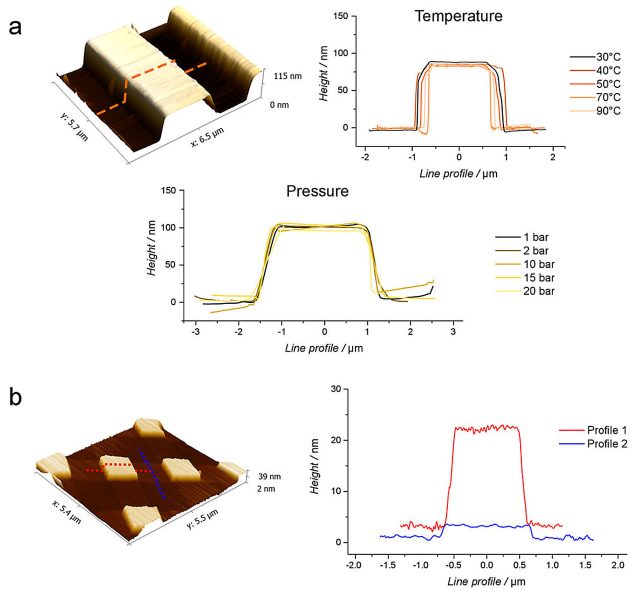

Figure 3. a) Si/SiO_2 calibration sample TGZ2 measured with the autoclave–inserted AFM instrument displaying the sensitivity at elevated *T* and *p*. The height profiles display the uniformity over the range of different conditions. b) Another Si/SiO_2 sample, TGQ1, measured at 113 °C and 13 bar, demonstrating the ability of the system to measure with high sensitivity at a combination of elevated *T* and *p*.

which can be explained by a blunted tip. As this tip was used for all scans and the profiles are nearly identical, the influence of the increased N_2 pressure on the scanning resolution seems to be negligible. Exposing the sample to both elevated *T* and *p* is also possible, as can be seen in Figure 3b. A different Si/SiO_2 (TGQ1) sample was measured at 113 °C and 13 bar. The red height profile 1 shows a $\Delta z \approx 20$ nm, and width of ~1.5 µm, in line with the grating. Even the small height difference displayed in the blue profile 2 was measured accurately with $\Delta z \approx 2$ nm (grating is 1.5 nm). Measuring at fixed conditions is more facile than scanning in a dynamic environment. The drift resulting from a change in conditions, but also the possible damage to the AFM tip when it is moving due to the thermal expansion of itself or the piezo crystals needs to be avoided. Hence, measuring the exact same location was not possible when studying *T* and *p* as variable because of the long stabilization times and resulting drift. In this work, the in-situ studies were performed on different spots, since the tip needed to be subtracted from the surface and the system stabilized for significant time when increasing *T* or *p*. In the future, in-situ studies using this AFM on fixed spots would be feasible and less challenging, as long as the system is stabilized on given conditions prior to scanning. These results create the possibility to use this system in time- or flow-resolved experiments for catalytic applications.

2.2. Thermal and Physical Stability of a HKUST-1 SURMOF

As showcase model, we have studied the changes in morphology when exposing a HKUST-1 thin-film to elevated *T* and *p* and the results are summarized in Figure 4. A quick observation when increasing *p* from 1 to 10 bar (20 °C) is the visible decrease in grain size (Figure 4, left column). A further increase in *p* (20 bar) does not equal a decrease in size as significant as seen for the previous pressure step, yet some size variations are visible. These observed *p* effects seem more pronounced at 20 °C than at increased *T* (Figure 4, middle and right column). Another significant effect is observed when applying *T* treatments. The height of the islands seems to decrease when *T* is increased, which is expressed by the color gradient scales at the top of each *p* set (Figure 4, top of columns). Furthermore, a striking observation is the lack of well-defined grains from measurements performed at 60 °C. A few particles are visible in the AFM micrograph at 1 bar (Figure 4, bottom right), however in a large area no SURMOF grains were visible from the AFM measurement. We also noticed two sharp edges in this micrograph, most likely due to partial removal of material using our AFM tip in contact mode in a previous scan. Since the scan settings are similar at all the different T and p, this observation might indicate a higher mobility of the HKUST-1 species at such temperatures. We do not experience similar scanning artefacts at lower T measurements. The subsequent scans at 60 °C and increased p (10, 20 bar, Figure 4, right column) performed at a different location of the sample show identical flat surface features. To show that possible tip–sample interactions are not significantly influencing the scanning resolution, AFM micrographs were measured on identical spots as for Figure 4. These data are shown in Figure S2. This is a strong indication of a

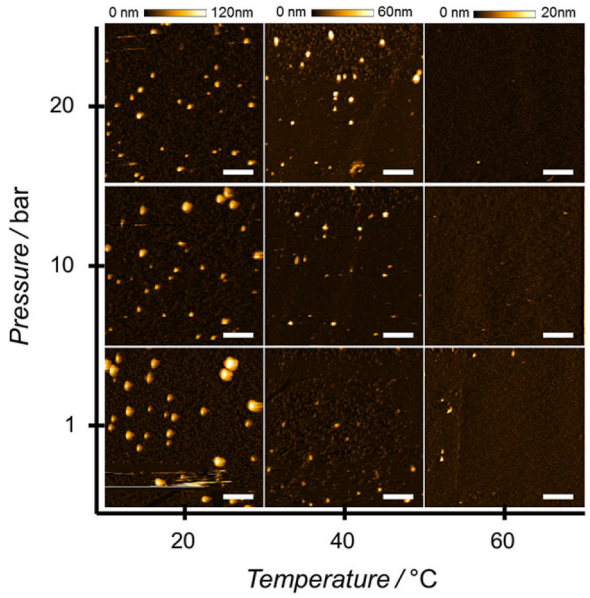

Figure 4. AFM topology maps of the HKUST-1 substrate measured in-situ at elevated temperatures (20, 40, 60 °C) and pressures (1, 10, 20 bar) using our autoclave-inserted AFM. Per temperature, the 3 different pressures were scanned prior to heating the autoclave to the following temperature overnight and repeating this process. As is easily observable from this figure, the amount of well-defined grains strongly decreases with higher temperatures. Also, the size of grains seems to decrease significantly during the first exposure to increased pressures. At 60 °C, well-defined particles were not observed. Note that the height scale bars are shown on top per temperature, resembling also the decrease in particle size when ramping up the temperature. White scale bars represent 2 μm.

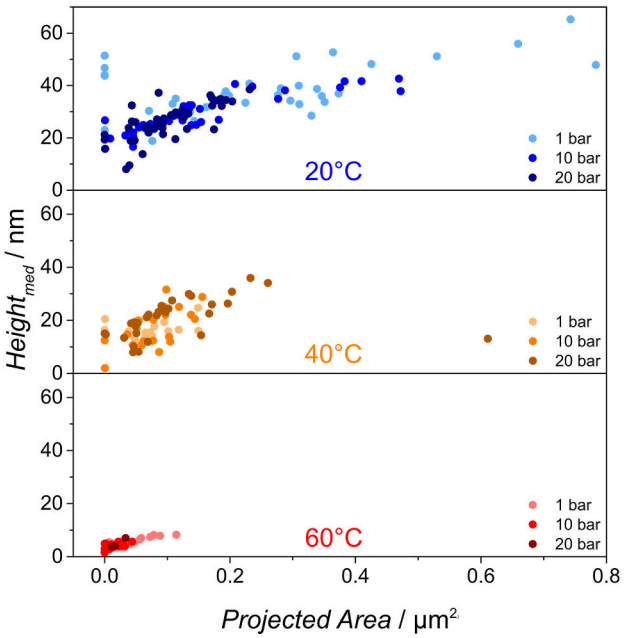

Figure 5. Distribution of all grains, displaying the projected area versus the median height of all individual grains found in Figure 4
All axes are kept identical to show the evolution of particles when increasing pressure and temperature.

potentially destructive effect on the SURMOF morphology under these *T* (and *p*) as scanned with the AFM.

Further analysis was performed on the particle size and number, to elucidate the different HKUST-1 features, as well as gain more insight into the mechanism behind the SURMOF morphology changes. To this end the grain base-area has been plotted versus the median height for all observed grains in all measured conditions and the results are summarized in Figure 5. Grains were selected by using a specific filter and we refer to the Supporting Information (e.g. Figure S3). The distributions of grains in Figure 5 confirm the island size decrease, in both area and height, when increasing *T* (from 20 to 40, then 60 °C): the average grain height decreases from 37.6 nm to 16.3 nm (64.6 %) and further down to 4.6 nm (87.8 %), respectively. Additionally, the observed size distribution illustrates the decreasing number of particles with increasing *T*, as well as *p*. One can imagine that for non-porous anchored islands, increasing *p* will introduce a mechanical strain onto the islands, thereby increasing the projected area, while decreasing the median height, that is, flattening. However, MOFs are extremely porous materials, and since a higher *p* would result in more molecules inside the pores and surrounding the grains, a MOF membrane should not be drastically expanded or compressed as long as the pores are accessible. Additionally, it is expected in the presented ranges of p that the HKUST-1 structure is not susceptible to irreversible strain.[51,52]

Figure 5 shows compression of the material when *p* is increased, and this effect is dominant during the initial rise from 1 to 10 bar (20 °C, median grain height decreases 22.1 %). At higher *T*, an increased *p* does not influence the grains that much. A noticeable compression can be observed at 40 °C, and an even smaller compression at 60 °C, but if thermal destructive interaction would have exposed the Au surface between these two conditions, the effects of *p* at 60 °C would only represent the compression of the Au grains. The compression at 40 °C from the increased *p* can be explained by considering the compression of the relatively flexible network of organic linkers; although the network might be porous, the linkers themselves become compressed by the N_2 gas, slightly decreasing the grain size. As the base area of the grains is not increasing at all, we can conclude that all grains are at least anchored to the Au surface and not flattened (spread out) under the influence of elevated *p*.

To complement the observations above and study the reversibility of the *T*,*p* effects, we performed ex-situ AFM measurements on samples exposed to either elevated *T* or elevated *p*, and the results are shown in Figure 6a and 6d, respectively. During the in-situ experiments, the SURMOF was first exposed to higher p prior to heating and was then scanned at elevated *T*. First, pressures are increased for the ex-situ measurements after which the samples are exposed to *T* (overnight) and measured afterwards at ambient conditions (Figure 6). It can be noted that increasing *T* decreases the grain size permanently, as is visualized for three prominent grains in Figure 6b. Over the whole temperature ramp, the average decrease in height from the traced grains (Figure 6a) is only 7.5 % (■ = 8.4 %, ● = 7.5 %, ▲ = 6.7 %). This decrease is smaller

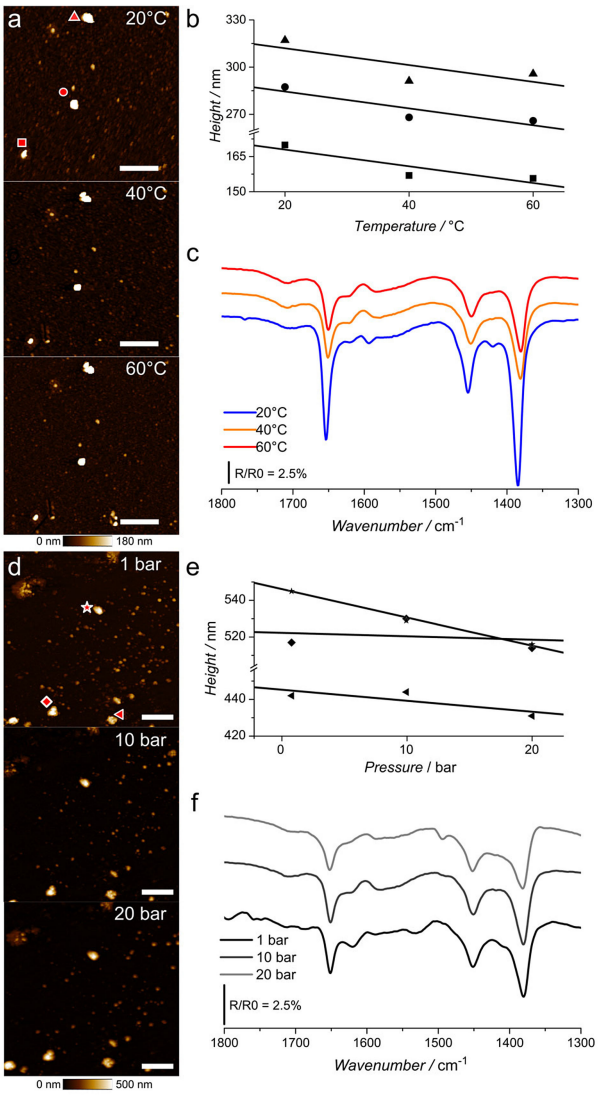

Figure 6. a) Ex-situ AFM measurements on identical spots of a HKUST-1 sample after exposure to elevated temperatures (measurements are at RT). b) Heights of 3 marked grains found in the AFM maps from (a) plotted after the thermal exposure. c) IRRAS spectra of corresponding sample, confirming the decomposition of HKUST-1. d) Similar sample, showing AFM maps after exposure to elevated pressures. e) Heights of the marked grains from (d) over time. f) IRRAS spectra recorded on this sample. White scale bars in AFM maps are 2 μm.

than the observed shrinkage in the in-situ measurements (Figures 4 and 5).

This difference can be due to two effects: i) the anisotropic thermal expansion of HKUST-1 (in fact shrinkage),[49] which is only observed when scanning at the given *T*, and thus not in our ex-situ set, and ii) the effect of scanning artefacts or tip-sample interactions. The scans obtained at 40 °C showed not any kind of distortion due to tip-interactions whatsoever. Therefore, it is reasonable that the shrinkage of grains is partly caused by the negative thermal expansion factor of the HKUST-1-gold substrate, as has been explicitly shown before by Wöll *et al.*[50] This idea has has been confirmed by comparing the decrease in feature sizes between in-situ (~65 %) and ex-situ (~10 %) experiments. Additionally, T effects decompose some of the SURMOF as there is a prolonged decrease in feature heights even after the exposure (in the range of 10 %) in the ex-situ experiment, as confirmed in the IRRAS spectra from Figure 6c (vide infra). The reversibility seems a contrast to the absence of features scanned in situ at 60 °C. We believe this is explained by Cu-BTC having a higher mobility, or weaker bonding to the gold substrate, making it susceptible to scanning artefacts in contact-mode, as the used AFM mode. The in-situ scanning at 60 °C was hampered noticeably compared to lower *T* measurements, and the removal of larger features is expected to be due to the interaction with the AFM- tip.

Interestingly, in earlier work we have observed a partial desorption of the SAM layer, binding the Cu-BTC to the gold surface, when synthesizing Cu-BTC SURMOFs at 50 °C.[53] Although the mentioned experiment was performed in liquid environment, the in-situ scans performed here at 60 °C might indicate the decreased stability of the Au–SAM–Cu-BTC interaction at such temperature ranges in general, weakening the anchoring of the MOF to the gold surface, and thus making it vulnerable to be "picked up" by an AFM tip. Nevertheless, we want to emphasize that this vulnerability must be dynamic and reversible, as reasoned from the ex-situ experiment and from the fact that bulk HKUST-1 is known to withstand such thermal exposure.[54] The *p* effect is different: the first decrease in grain size when exposed to 10 bar in-situ at 20 °C (Figures 3 and 4) was 22.1 %, and except for this specific *p* increment step, the further decrease in grain sizes were small. Comparing this to the grains observed in Figure 6d, we see a fairly random and small decrease in grain height, with an average decrease in grain height of only 2.8 % (Figure 6e, * = 5.3 %, ◆ = 0.6 %, ◀ = 2.6 %). This is in line with the in-situ scans where, except for the first increase, the grain height decreased slightly, which we attributed to the physical compression of the organic linkers and should thus be reversible.

Understanding the chemical changes which are unavoidably linked to the morphological effects is a necessity in explaining the stability of HKUST-1 thin-films under these conditions. Thus, to gain more chemical insights into the morphological changes of the SURMOFs, infrared reflection absorption spectroscopy (IRRAS) spectra (Figure 6c, f) were recorded prior to- and after (*T* and *p*) treatments on the samples used for the ex-situ AFM analysis. The spectrum of the fresh HKUST-1 samples (Figure 6c, blue line, Figure 6f, black line) show characteristic HKUST-1 features: peaks at 1650 cm^{-1} and 1380 cm^{-1} represent the asymmetric and symmetric $-COO^-$ vibration, respectively. The peak at 1450 cm^{-1} is ascribed to benzene breathing modes of the linker molecule.[48,49,55,56] IRRAS is a semi-quantitative analysis method, that is, lower relative intensities between spectra indicate lower amounts of material present. As such, the drop in spectral intensity seen for both *T* treated samples (40 °C, 60 °C, Figure 6c, orange and red line respectively) underlines the distortion of the corresponding Cu-BTC interaction upon increasing *T*. The peak position of the υ_{sym} and υ_{asym} COO^- stretch is red-shifted, showing a change in coordination of the COO^- to the Cu cluster. Additionally, the band ~1700 cm^{-1}, caused by C=O stretch, i.e. from the uncoordinated acid groups of BTC linkers, is slightly in-

creased.[53] The effect of *p* is less pronounced, in line with our AFM analysis. There is a very slight decrease in intensity for the Cu-BTC bands with increasing *p*, but there is no red-shift observed for these peaks and the band around 1700 cm^{-1} did not gain intensity, reflecting the physical robustness of our HKUST-1 thin-film.

3. Conclusions

Using a tailor-made autoclave-inserted AFM, we were able to obtain micrographs at *T* up to ~110 °C and *p* up to ~20 bar. As a showcase model, we have obtained for the first time insights into the stability of SURMOF thin-films, in-situ, at elevated *T* and *p* using AFM. In order to further improve our understanding of the observed processes, we have complemented the in-situ dataset with ex-situ AFM and observed spectroscopic changes using IRRAS. A SURMOF consisting of 5 layers HKUST-1 is shown to be strongly affected at elevated *T* and much less at elevated p. Although these morphological changes turned out to be mostly reversible, the height of MOF grains decreased with ~65% when heated up to 40 °C and ~22% when put under 10 bar.

Using the developed in-situ autoclave-inserted AFM to measure the HKUST-1 sample at 60 °C was nearly impossible, and resulting images show an absence of surface features characteristic to the measured sample. The interaction between AFM tip and MOF material must be too strong, possibly due to an increased mobility in the MOF framework, as the ex-situ AFM scans showed that most of the decrease was reversible. Nevertheless, IRRAS measurements confirm the decomposition of the HKUST-1 framework at elevated temperatures. The physical stability seems to be better, as both *in*-situ and ex-situ measurements only exposed slight decreases in grain height, complemented by a minimal change in the IRRAS spectra.

Concluding from this work, it is therefore important to understand that HKUST-1 thin-films are not completely stable at elevated temperatures. Nevertheless, their stability at higher p is promising for possible applications in gas-sensing, separation as well as heterogeneous catalysis. Furthermore, using HKUST-1 as a showcase model, we have shown that in-situ AFM at elevated *T* and *p* is a powerful characterization tool to study surface processes, changes and mechanisms, not only limited to MOFs, but also other thin(-film) nanomaterials that require such experimental conditions for their possible (catalytic) applications.

Experimental Section

Chemicals and Materials

The following chemicals were used: 16-mercaptohexadecanoic acid (MHDA) (99%, Sigma-Aldrich), absolute ethanol (99.5%, Acros), Cu(II)acetate (98%, Aldrich), trimesic acid or benzene tricarboxylic acid (BTC) (95%, Aldrich) and acetic acid (Ac) (99.5%, Acros). Substrates of 60 nm Au on Si, with a 5 nm Ge adhesion layer (provided by AMOLF, Amsterdam) were functionalized with a Self-Assembled Monolayer (SAM) by immersing in 20 μM 16-mercaptohexadecanoic acid solution (5% acetic acid in ethanol) for 48 h. Substrates were rinsed in washing solution (5% acetic acid in ethanol) and dried in flowing N_2 prior to use. SURMOF thin-films were synthesized using the Layer-by-Layer (LbL) technique.[48] Purposefully, a low degree of washing was utilized to prevent optimally coordinated LbL growth and ensure the inhomogeneity of the surface visible in AFM. HKUST-1 thin-films were deposited in cycles where one cycle consisted of successively placing Au-MHDA substrates in separate ethanolic 1 mM precursor solutions of $CuAc_2$ (30 min) and BTC solution (60 min). After each immersion ($CuAc_2$, BTC) the substrate was washed for 5 s. This process was repeated for 5 cycles. All syntheses were performed at room temperature.

Atomic Force Microscopy, Protocols, and Data Analysis

The autoclave AFM was custom built by Optics 11 (Amsterdam, the Netherlands) and mounted on a vibration isolation platform (150BM-1, minus k Technology). This was placed into a cabinet which was both acoustically and thermally isolated. The cantilever deflection signal is processed by an OP1550v2 interferometer (Optics 11) and was both fed back to a computer and to the AFM control unit for feedback control. The AFM uses sample scanning based on a 2D bender piezo and a z-finepiezo. In the control unit the z piezo amplifier (fast) a PDL200 driver (PiezoDrive) is used and the *x* and *y* piezo amplifiers (slow) are NDR6110 Single Channel Dynamic Drivers (Noliac). Processing of the signals and feedback into the system are carried out by a Signal Ranger SR-MK3-PRO extended with a SR-A810-V2 expansion board (both Soft dB) dedicated for use in SPM systems. Tip-sample approach (coarse and fine) is done by moving the probe with a DC-Mike High-Resolution Linear Actuator (M-227.10, PI) to the stage controlled by the GXSM software. Heating is performed using a power supply (SM400-AR-8, Delta Elektronica) and 4 standard cartridge heaters (diam. $^1/_4$'', length 2'', Acim Jouanin) as heating elements in the autoclave wall. As a temperature sensor a Pt-100 sensor (TRC-P1-A-1, SensorData) is used. Temperature readout is performed by a Eurotherm readout device (32H8I 1/8 DIN Alarmunit) both coupled to a computer to log their read out and to control the power supply. A digital pressure transmitter (HD 9408T, Delta Ohm) in combination with a 4 Digital process indicator (HD9022, Delta Ohm) is used to log the pressure in the cell. An overview of the complete setup, some photographs as well as additional experimental details can be found in the Supporting information.

The in-situ AFM measurements on the SURMOF samples were performed using the following protocol: the HKUST-1 substrate was fixed in the autoclave AFM using two clamps. The autoclave was then closed airtight and connected to a N_2-line. The isolation box around the autoclave-AFM was closed, and not opened until all scans were performed, ensuring minimum fluctuations in temperature. AFM topology maps were scanned in contact mode, using a scan rate of 4000 nm s^{-1}. The measured scan range was 10×10 μm. First, the sample was scanned at ambient conditions. When changing *T* and/or *p*, the AFM-probe was retracted a few steps from the surface, and the pressure was increased to 10, and finally 20 bar. The system was then vented back to 1 bar. After the scans at different pressures, performed on one day, the cell was heated overnight to 40 °C and finally 60 °C. For those temperatures, the substrate was scanned at the same pressures in a similar manner. After scanning at 60 °C and 20 bar the tip was fully retracted, the autoclave was cooled down and vented, and the substrate was removed for post-experiment analysis.

Ex-situ AFM images were recorded on an NT-MDT NTEGRA Spectra system using HA_NC etalon (force constant: 3.5 N/m) probes, in tapping mode at a resonance frequency of 140 kHz. To study the

effect of pressure (ex-situ), a fresh HKUST-1 film was marked with a scalpel, and alternatively put under pressure (10 or 20 bar, 1 h) in the autoclave-AFM system and scanned at marked position with the commercial AFM. To study the effect of temperature (ex-situ), a fresh HKUST-1 film was marked and scanned in similar fashion, but the sample was left in the autoclave-AFM at elevated temperatures (40 °C and 60 °C) for approximately 17 h before being transferred to and scanned with our commercial system. The obtained AFM maps were then post-treated and analyzed in an identical manner as the in-situ AFM experiments (see the Supporting information for more details).

Infrared Reflection Absorption Spectroscopy

InfraRed Reflection Absorption Spectroscopy (IRRAS) spectra were recorded using a PelkinElmer Spectrum One infrared spectrometer equipped with grazing angle specular reflectance accessory (Specac) and a mercury cadmium telluride (MCT) detector. A spectrum was collected by averaging 50 spectra in the 1300–1800 cm^{-1} range with a resolution of 4 cm^{-1}. To prevent signal hindrance of adsorbed water, the sample chamber was purged with N_2. Grazing incidence angles of 80° were used and the incident beam was vertically polarized.

Acknowledgements

This work is supported by a Netherlands Organization of Scientific Research (NWO) Gravitation program (Netherlands Center for Multiscale Catalytic Energy Conversion, MCEC) and a European Research Council (ERC) Advanced Grant (no. 321140).

Conflict of Interest

The authors declare no conflict of interest.

Keywords: atomic force microscopy · autoclave measurements · catalyst stability · metal-organic frameworks · scanning probe microscopy

[1] G. Binnig, C. F. Quate, C. Gerber, *Phys. Rev. Lett.* **1986**, *56*, 930–933.
[2] G. Binnig, H. Rohrer, C. Gerber, E. Weibel, *Phys. Rev. Lett.* **1982**, *49*, 57–61.
[3] G. Binnig, H. Rohrer, C. Gerber, E. Weibel, *Appl. Phys. Lett.* **1982**, *40*, 178–180.
[4] G. Haugstad, *Atomic Force Microscopy: Understanding Basic Modes and Advanced Applications*, Wiley, Weinheim, **2012**.
[5] O. Marti, M. Amrein, *STM and SFM in Biology*, Elsevier Science, Burlington, **2012**.
[6] J. K. H. Hörber, M. J. Miles, *Science* **2003**, *302*, 1002–1005.
[7] D. P. Allison, N. P. Mortensen, C. J. Sullivan, M. J. Doktycz, *Wiley Interdiscip. Rev. Nanomed. Nanobiotechnol.* **2010**, *2*, 618–634.
[8] L. S. Dorobantu, M. R. Gray, *Scanning* **2010**, *32*, 74–96.
[9] B. Bhushan, Ed., *Scanning Probe Microscopy in Nanoscience and Nanotechnology*, Springer, Berlin, **2010**.
[10] V. V. Tsukruk, S. Singamaneni, *Scanning Probe Microscopy of Soft Matter: Fundamentals and Practices*, Wiley-VCH, Weinheim, **2011**.
[11] F. Giessibl, *Rev. Mod. Phys.* **2003**, *75*, 949–983.
[12] A. I. Lupulescu, J. D. Rimer, *Science* **2014**, *344*, 729–732.
[13] M. H. Shete, M. Kumar, D. Kim, N. Rangnekar, D. Xu, B. Topuz, K. V. Agrawal, E. Karapetrova, B. Stottrup, S. Al-Thabaiti, S. Basahel, K. Narasimharao, J. D. Rimer, M. Tsapatsis, *Angew. Chem. Int. Ed.* **2017**, *56*, 535–539; *Angew. Chem.* **2017**, *129*, 550–554
[14] P. B. Rasmussen, B. L. M. Hendriksen, H. Zeijlemaker, H. G. Ficke, J. W. M. Frenken, *Rev. Sci. Instrum.* **1998**, *69*, 3879–3884.
[15] C. T. Herbschleb, P. C. van der Tuijn, S. B. Roobol, V. Navarro, J. W. Bakker, Q. Liu, D. Stoltz, M. E. Cañas-Ventura, G. Verdoes, M. A. van Spronsen, M. Bergman, L. Crama, I. Taminiau, A. Ofitserov, G. J. C. van Baarle, J. W. M. Frenken, *Rev. Sci. Instrum.* **2014**, *85*, 083703.
[16] S. B. Roobol, M. E. Cañas-Ventura, M. Bergman, M. A. van Spronsen, W. G. Onderwaater, P. C. van der Tuijn, R. Koehler, A. Ofitserov, G. J. C. van Baarle, J. W. M. Frenken, *Rev. Sci. Instrum.* **2015**, *86*, 033706.
[17] M. A. van Spronsen, G. J. C. van Baarle, C. T. Herbschleb, J. W. M. Frenken, I. M. N. Groot, *Catal. Today* **2015**, *244*, 85–95.
[18] B. L. M. Hendriksen, S. C. Bobaru, J. W. M. Frenken, *Surf. Sci.* **2004**, *552*, 229–242.
[19] C. T. Herbschleb, S. C. Bobaru, J. W. M. Frenken, *Catal. Today* **2010**, *154*, 61–67.
[20] V. Navarro, M. A. van Spronsen, J. W. M. Frenken, *Nat. Chem.* **2016**, *8*, 929–934.
[21] G. Ertl, H. Knözinger, F. Schüth, J. Weitkamp, Eds., *Handbook of Heterogeneous Catalysis*, Wiley-VCH, Weinheim, **2008**.
[22] J. Cejka, A. Corma, S. Zones, Eds., *Zeolites and Catalysis: Synthesis, Reactions and Applications*, Wiley-VCH, Weinheim, **2010**.
[23] O. M. Yaghi, H. Li, *J. Am. Chem. Soc.* **1995**, *117*, 10401–10402.
[24] H. Li, M. Eddaoudi, M. O'Keeffe, O. M. Yaghi, *Nature* **1999**, *402*, 276–279.
[25] S. T. Meek, J. A. Greathouse, M. D. Allendorf, *Adv. Mater.* **2011**, *23*, 249–267.
[26] D. Farrusseng, Ed., *Metal-Organic Frameworks: Applications from Catalysis to Gas Storage*, Wiley-VCH, Weinheim, **2011**.
[27] P. Kumar, K. Vellingiri, K. Kim, R. J. C. Brown, M. J. Manos, *Microporous Mesoporous Mater.* **2017**, *253*, 251–265.
[28] J. Liang, Z. Liang, R. Zou, Y. Zhao, *Adv. Mater.* **2017**, *29*, 1701139.
[29] T. D. Bennett, A. K. Cheetham, A. H. Fuchs, F. Coudert, *Nat. Chem.* **2017**, *9*, 11–16.
[30] K. L. Mulfort, O. K. Farha, C. D. Malliakas, M. G. Kanatzidis, J. T. Hupp, *Chem. Eur. J.* **2010**, *16*, 276–281.
[31] A. Betard, R. A. Fischer, *Chem. Rev.* **2012**, *112*, 1055–1083.
[32] D. Zacher, O. Shekhah, C. Wöll, R. A. Fischer, *Chem. Soc. Rev.* **2009**, *38*, 1418–1429.
[33] O. Shekhah, J. Liu, R. A. Fischer, C. Wöll, *Chem. Soc. Rev.* **2011**, *40*, 1081–1106.
[34] K. L. Mulfort, O. K. Farha, C. D. Malliakas, M. G. Kanatzidis, J. T. Hupp, *Chem. Eur. J.* **2010**, *16*, 276–281.
[35] E. Biemmi, C. Scherb, T. Bein, *J. Am. Chem. Soc.* **2007**, *129*, 8054–8055.
[36] S. S. Chui, *Science* **1999**, *283*, 1148–1150.
[37] J.-R. Li, J. Sculley, H.-C. Zhou, *Chem. Rev.* **2012**, *112*, 869–932.
[38] S. Bordiga, L. Regli, F. Bonino, E. Groppo, C. Lamberti, B. Xiao, P. S. Wheatley, R. E. Morris, A. Zecchina, *Phys. Chem. Chem. Phys.* **2007**, *9*, 2676–2685.
[39] D. Farrusseng, C. Daniel, C. Gaudillère, U. Ravon, Y. Schuurman, C. Mirodatos, D. Dubbeldam, H. Frost, R. Q. Snurr, *Langmuir* **2009**, *25*, 7383–7388.
[40] J. Liu, Y. Wang, A. I. Benin, P. Jakubczak, R. R. Willis, M. D. LeVan, *Langmuir* **2010**, *26*, 14301–14307.
[41] J. Moellmer, A. Moeller, F. Dreisbach, R. Glaeser, R. Staudt, *Microporous Mesoporous Mater.* **2011**, *138*, 140–148.
[42] H. Chen, L. Wang, J. Yang, R. T. Yang, *J. Phys. Chem. C* **2013**, *117*, 7565–7576.
[43] X. Yan, S. Komarneni, Z. Zhang, Z. Yan, *Microporous Mesoporous Mater.* **2014**, *183*, 69–73.
[44] O. Shekhah, H. Wang, S. Kowarik, F. Schreiber, M. Paulus, M. Tolan, C. Sternemann, F. Evers, D. Zacher, R. A. Fischer, C. Wöll, *J. Am. Chem. Soc.* **2007**, 129, 15118–15119.
[45] D. Zacher, A. Baunemann, S. Hermes, R. A. Fischer, *J. Mater. Chem.* **2007**, *17*, 2785–2792.
[46] O. Shekhah, H. Wang, M. Paradinas, C. Ocal, B. Schüpbach, A. Terfort, D. Zacher, R. A. Fischer, C. Wöll, *Nat. Mater.* **2009**, *8*, 481–484.
[47] D. Zacher, K. Yusenko, A. Bétard, S. Henke, M. Molon, T. Ladnorg, O. Shekhah, B. Schüpbach, T. de los Arcos, M. Krasnopolski, M. Meilikhov, J. Winter, A. Terfort, C. Wöll, R. A. Fischer, *Chem. Eur. J.* **2011**, *17*, 1448–1455.
[48] G. Delen, Z. Ristanovic, L. D. B. Mandemaker, B. M. Weckhuysen, *Chem. Eur. J.* **2017**, *23*, 187–195.

[49] Y. Wu, A. Kobayashi, G. J. Halder, V. K. Peterson, K. W. Chapman, N. Lock, P. D. Southon, C. J. Kepert, *Angew. Chem. Int. Ed.* **2008**, *47*, 8929–8932; *Angew. Chem.* **2008**, *120*, 9061–9064.
[50] Z. Wang, P. G. Weidler, C. Azucena, L. Heinke, C. Wöll, *Microporous Mesoporous Mater.* **2016**, *222*, 241–246.
[51] J. C. Tan, A. K. Cheetham, *Chem. Soc. Rev.* **2011**, *40*, 1059–1080.
[52] M. D. Allendorf, R. J. T. Houk, L. Andruszkiewicz, A. A. Talin, J. Pikarsky, A. Choudhury, K. A. Gall, P. J. Hesketh, *J. Am. Chem. Soc.* **2008**, *130*, 14404–14405.
[53] L. D. B. Mandemaker, M. Filez, G. Delen, H. Tan, X. Zhang, D. Lohse, B. M. Weckhuysen, *J. Phys. Chem. Lett.* **2018**, *9*,1838-1844.
[54] K.-S. Lin, A. K. Adhikari, C.-N. Ku, C.-L. Chiang, H. Kuo, *Int. J. Hydrogen Energy* **2012**, *37*, 13865–13871.
[55] L. Pan, Z. Ji, X. Yi, X. Zhu, X. Chen, J. Shang, G. Liu, R. W. Li, *Adv. Funct. Mater.* **2015**, *25*, 2677–2685.
[56] E. Borfecchia, S. Maurelli, D. Gianolio, E. Groppo, M. Chiesa, F. Bonino, C. Lamberti, *J. Phys. Chem. C* **2012**, *116*, 19839–19850.

Manuscript received: April 1, 2018
Accepted Article published: June 6, 2018
Version of record online: June 22, 2018